

See discussions, stats, and author profiles for this publication at: <https://www.researchgate.net/publication/330792814>

# Magnetic resonance imaging radiomic feature analysis of radiation-induced femoral head changes in prostate cancer radiotherapy

Article in *Journal of Cancer Research and Therapeutics* · March 2019

DOI: 10.4103/jcrt.JCRT\_172\_18

CITATIONS

12

READS

157

6 authors, including:



**Hamid Abdollahi**

Kerman University of Medical Sciences

80 PUBLICATIONS 488 CITATIONS

[SEE PROFILE](#)



**Isaac Shiri**

University of Geneva

61 PUBLICATIONS 340 CITATIONS

[SEE PROFILE](#)



**Bahram Mofid**

Shahid Beheshti University of Medical Sciences

81 PUBLICATIONS 238 CITATIONS

[SEE PROFILE](#)



**Mohsen Bakhshandeh**

Shahid Beheshti University of Medical Sciences

55 PUBLICATIONS 156 CITATIONS

[SEE PROFILE](#)

Some of the authors of this publication are also working on these related projects:



Evaluation of accuracy of dosimetry calculations of IMRT & 3DCRT in treatment planning systems of Prostate cancer patients [View project](#)



Translational research on nanocurcumin as a radio- and/or chemo-modulator [View project](#)

# Journal of Cancer Research and Therapeutics

Volume 15, Supplement Issue 1 - 2019



Official Journal of  
Association of Radiation Oncologist of India

Full Text Online at: [www.cancerjournal.net](http://www.cancerjournal.net)

Impact Factor® as reported in the 2017  
Journal Citation Reports®  
(Clarivate Analytics, 2018): 0.842

# Magnetic resonance imaging radiomic feature analysis of radiation-induced femoral head changes in prostate cancer radiotherapy

Hamid Abdollahi<sup>1</sup>,  
Seied Rabi  
Mahdavi<sup>1,2</sup>,  
Isaac Shiri<sup>3,4</sup>,  
Bahram Mofid<sup>5</sup>,  
Mohsen  
Bakhshandeh<sup>6</sup>,  
Kazem Rahmani<sup>7</sup>

<sup>1</sup>Department of Medical Physics, School of Medicine, Iran University of Medical Sciences, <sup>2</sup>Radiation Biology Research Center, Iran University of Medical Sciences, <sup>3</sup>Research Center for Molecular and Cellular Imaging, Tehran University of Medical Sciences, <sup>4</sup>Department of Biomedical and Health Informatics, Rajaei Cardiovascular, Medical and Research Center, Iran University of Medical Sciences, <sup>5</sup>Department of Clinical Oncology, Shohada-e-Tajrish Medical Center, Shahid Beheshti University of Medical Sciences, <sup>6</sup>Department of Radiation Technology, Allied Medicine Faculty, Shahid Beheshti University of Medical Sciences, <sup>7</sup>Department of Biostatistics, School of Public Health, Iran University of Medical Sciences, Tehran, Iran

**For correspondence:** Dr. Seied Rabi Mahdavi, Department of Medical Physics, School of Medicine, Iran University of Medical Sciences, Tehran, Iran. E-mail: srmahdavi@hotmail.com  
Dr. Hamid Abdollahi, Department of Medical Physics, School of Medicine, Iran University of Medical Sciences, Junction of Shahid Hemmat and Shahid Chamran Expressways, Tehran 14496, Iran. E-mail: hamid\_rbp@yahoo.com

## ABSTRACT

**Background and Purpose:** As a feasible approach, radiotherapy has a great role in prostate cancer (Pca) management. However, Pca patients have an increased risk of femoral head damages including fractures after radiotherapy. The mechanisms of these complications are unknown and time of manifestations is too long; however, they may be predicted by early imaging. The main purpose of this study was to assess the early changes in femoral heads in Pca patients treated with intensity-modulated radiation therapy (IMRT) using multiparametric magnetic resonance imaging (mpMRI) radiomic feature analysis.

**Materials and Methods:** Thirty Pca patients treated with IMRT were included in the study. All patients underwent two mpMRI pre- and postradiotherapy. Thirty-four robust radiomic features were extracted from T1, T2, and apparent diffusion coefficient (ADC) obtained from diffusion-weighted images. Wilcoxon signed-rank test was performed to assess the significance of the change in the mean T1, T2, and ADC radiomic features postradiotherapy relative to preradiotherapy values. The percentage change values were normalized based on the natural logarithm base ten. Features were also ranked based on their median changes.

**Results:** Sixty femoral heads were analyzed. All radiomic features have undergone changes. Significant postradiotherapy radiomic feature changes were observed in 20 and 5 T1- and T2-weighted radiomic features, respectively ( $P < 0.05$ ). ADC features did not vary significantly postradiotherapy. The mean radiation dose received by femoral heads was 40 Gy. No fractures were observed within the follow-up time. Different features were found as high ranked among T1, T2, and ADC images.


**Conclusion:** Early structural change analysis using radiomic features may contribute to predict postradiotherapy fracture in Pca patients. These features can be identified as being potentially important imaging biomarkers for predicting radiotherapy-induced femoral changes.

**KEY WORDS:** Feature changes, femoral head, magnetic resonance imaging, prostate cancer, radiomics, radiotherapy

## INTRODUCTION

Prostate cancer (Pca) is the most common malignancy among men. As a feasible approach, radiotherapy has a great role in Pca management. However, normal tissue toxicities during or after radiotherapy remain the main limiting factors with negative impacts on

patient's quality of life.<sup>[1]</sup> Radiation-associated femoral head/neck toxicities including fractures, cortical bone thinning, and necrosis are complications which may occur months to years after radiotherapy.<sup>[2,3]</sup> Previous studies have indicated that femoral insufficiency fracture is significantly higher in patients who receive pelvic irradiation.<sup>[4,5]</sup> Femoral head fractures due to radiotherapy are associated with high morbidity and significant mortality.

Access this article online	
Website: <a href="http://www.cancerjournal.net">www.cancerjournal.net</a>	Quick Response Code: 
DOI: 10.4103/jcrt.JCRT_172_18	

This is an open access journal, and articles are distributed under the terms of the Creative Commons Attribution-NonCommercial-ShareAlike 4.0 License, which allows others to remix, tweak, and build upon the work non-commercially, as long as appropriate credit is given and the new creations are licensed under the identical terms.

For reprints contact: [reprints@medknow.com](mailto:reprints@medknow.com)

**Cite this article as:** Abdollahi H, Mahdavi SR, Shiri I, Mofid B, Bakhshandeh M, Rahmani K. Magnetic resonance imaging radiomic feature analysis of radiation-induced femoral head changes in prostate cancer radiotherapy. *J Can Res Ther* 2019;15:S11-9.

Although the mechanisms by which radiation induces bone damages have been studied extensively, they remain unclear. Some studies have revealed that radiotherapy changes the biomechanical properties of bones including matrix embrittlement.<sup>[6]</sup> Furthermore, previous research has shown that radiotherapy suppresses normal osteoblast proliferation.<sup>[7]</sup> It was also shown that radiation sensitizes bone cells to apoptosis.<sup>[8]</sup>

Magnetic resonance imaging (MRI) can be utilized as a feasible modality to detect bone abnormalities.<sup>[9,10]</sup> MR image sequences including T1-weighted (T1W), T2W, and diffusion-weighted (DW) are of importance in bone disease diagnosis.<sup>[11]</sup> On the other hand, apparent diffusion coefficient (ADC), which is proportional to the cellular density, ratio of extracellular and intracellular components, and also soluble intracellular macromolecules, has been used in differentiating and detecting bone pathologies.<sup>[12]</sup>

Recent advances in image analysis and biomarker research have produced powerful platforms for diagnosis, prognosis prediction, and therapeutic management of diseases.<sup>[13]</sup> As an important current and future-based science, radiomics have been used to quantify tumor characteristics and also

radiotherapy-associated clinical manifestations.<sup>[14,15]</sup> It is a newly accepted branch of image processing which aims to correlate high-dimensional imaging features with clinical data. Furthermore, in radiomic literature, changes in different imaging features were correlated with radiation dose<sup>[16]</sup> and clinical observations such as tissue shrinkage or density changes and hearing loss.<sup>[17-19]</sup>

In the present study, for the first time, we applied radiomic feature analysis on MR images with the aim to assess changes in femoral head after the course of radiotherapy.

**MATERIAL AND METHODS**

Our radiomic flowchart is depicted in Figure 1. From Figure 1, our study is composed of four continuing phases including (1) imaging and segmentation, (2) image preprocessing, (3) feature extraction, and (4) data analysis.

**Study participants**

In this prospective study, to test how radiotherapy induces femoral head changes, we conducted an MR image radiomic

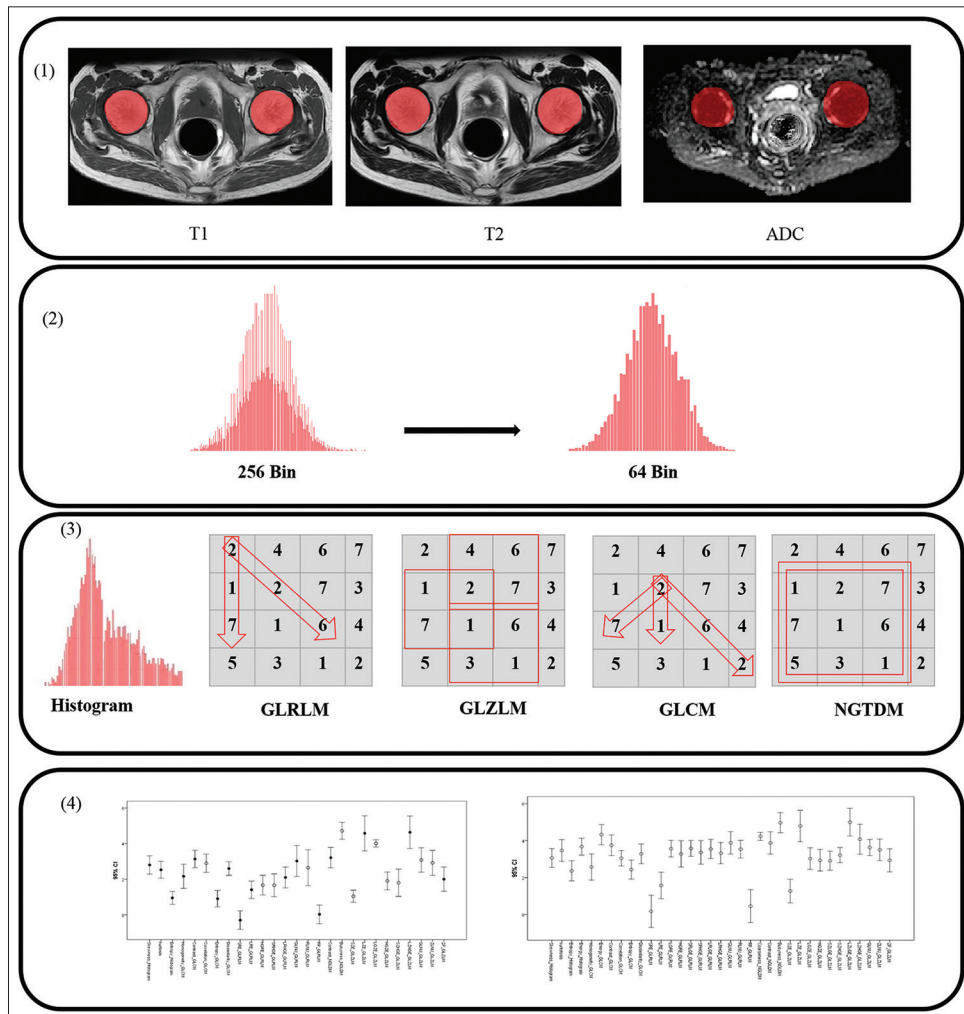


**Figure 1:** Radiomic flowchart

feature analysis. Between January 2015 and September 2016, we enrolled 30 Pca patients, with different Gleason scores, in accordance with the ethical standards of the responsible committee on human experimentation and in compliance with the 1975 Declaration of Helsinki and its revision in 2000. Because this work was conducted as prospective, all participants gave informed consent before enrollment. Patients were treated with intensity-modulated radiation therapy (IMRT), with 70.6 Gy in 25 fractions and treatment was delivered with multileaf collimators using 9 coplanar or noncoplanar, nonuniform beams. All planning was performed using Eclipse treatment planning system (Varian Medical Systems). In the plans, both right and left femoral heads were delineated as organs at risk and their mean radiation doses were obtained from TPS and their relevant dose volume histograms. The patients were followed for 6 months to 1 year for postradiotherapy bone damages. The patient details are shown in Table 1.

**Magnetic resonance imaging**

All participants underwent two MRI scans, pre- and postradiotherapy. The mean time for MR scanning after radiotherapy was 3 months. Both pre- and postradiotherapy MRI scans included T1W, T2W, and DW imaging protocols. All studies were performed using 1.5 Tesla MRI machines (Siemens and Philips) equipped with endorectal and phased-array coils. The imaging protocols are shown in

**Table 1: Patient details participating in this study**

Characteristic	Value	
Number of patients (n)	30	
Age (years)		
Mean	68.6	
Range	51-80	
PSA level (ng/ml), before RT		
Mean	24.73	
Range	5-97	
Radiotherapy technique/dose (n)		
IMRT	70.6 in 25 fraction	
Gleason score (n)		
6	10	
7	9	
8	4	
9	4	
10	3	
Femoral head dose	Right	Left
Mean	40.9	39.7
Range	0.9-52.6	23.6-52.7

PSA=Prostate-specific antigen, IMRT=Intensity-modulated radiation therapy, RT=Radiation therapy

**Table 2: Imaging protocols from two scanners**

Scanners/imaging protocol	Siemens			Philips		
	T1w	T2w	DW	T1w	T2w	DW
Slice thickness (mm)	3	3	3.5	3.5	3.5	5
Repetition time (TR) (ms)	563	3000	3900	509	3065	4600
Echo time (TE) (ms)	14	101	100	10	80	90
Acquisition matrix	256×224	256×205	150×150	300×278	300×262	120×122
b-value (s/mm <sup>2</sup> )	-	-	1200	-	-	1000

Table 2. For each patient, MR image protocols were the same in pre- and postradiotherapy scans. ADC was automatically calculated by the imager software with the use of the *b-values* reported in Table 2.

**Radiomic features**

Multiple radiomic feature sets including histogram, co-occurrence gray-level matrix (GLCM), gray-level run length matrix, gray-level zone length matrix, and neighborhood gray-level difference matrix were applied on MR images. The robustness of these features was tested in previous studies.<sup>[20-22]</sup> Table 3 shows the details of these features. For radiomic analysis, femoral heads were segmented in each slice on T1W, T2W, and ADC images and obtained three-dimensional (3D) regions of interest were used for feature analysis. To reduce interobserver variability, all femoral heads were segmented by an experienced radiation oncologist physicist. All segmentations were done manually and verified by an experienced radiologist (more than 10 years' experiences in musculoskeletal imaging). Before feature extraction, all image intensities were discretized to 64 gray levels, in order to image noise reduction, increasing sensitivity, and normalizing the intensities across all the patients.

**Statistical analysis**

All statistical analyses were performed using STATA (Version 11.1, SE Texas). Wilcoxon signed-rank test was performed to assess the significance of the change in mean T1W, T2W, and ADC radiomic features postradiotherapy relative to preradiotherapy values. Statistical significance was assumed if *P* < 0.05 and all reported *P* values are two sided. The percentage changes of the postradiotherapy to the preradiotherapy for all radiomic features were also calculated to show the relative changes postradiation. The percentage change values were normalized based on the natural logarithm base 10. This ensured that the different parameter values were in a comparable range of values when quantifying differences between pre- and postradiotherapy.

**RESULTS**

All radiomic features in T1W/T2W/ADC images had difference between pre- and postradiotherapy. Normalized percentage changes with 95% confidence intervals of these features are shown in Figures 2-4. We also showed the MRI radiomic features ranking in Table 4. Features ranked in the descending order based on the median values. High rank features showing

**Table 3: Radiomic features**

Features	Complete name	Equation
Histogram		
Skewness	-	$\frac{\frac{1}{N} \sum_{i=1}^N (X(i) - \bar{X})^3}{\left(\frac{1}{N} \sum_{i=1}^N (X(i) - \bar{X})^2\right)^{\frac{3}{2}}}$
Energy	-	$\sum_j \{p(i)\}^2$
Kurtosis	-	$\frac{\frac{1}{N} \sum_{i=1}^N (X(i) - \bar{X})^4}{\left(\frac{1}{N} \sum_{i=1}^N (X(i) - \bar{X})^2\right)^2}$
Entropy	-	$-\sum_i p(i) \log(p(i))$
GLCM		
Energy	-	$\sum_i \sum_j \{p(i, j)\}^2$
Contrast	-	$\sum_{n=0}^{Ng-1} n^2 \left\{ \sum_{i=1}^{Ng} \sum_{j=1}^{Ng} p(i, j) \right\}$
Entropy	-	$-\sum_i \sum_j p(i, j) \log(p(i, j))$
Homogeneity	-	$\sum_{i=1}^{G_{max}} \left\{ \sum_{j=1}^{G_{max}} \left\{ \frac{1}{1+(i-j)^2} \cdot p_{i,j} \right\} \right\}$
Dissimilarity	-	$\sum_{i=1}^{G_{max}} \left\{ \sum_{j=1}^{G_{max}} \{ i-j  \cdot p_{i,j}\} \right\}$
Correlation	-	$\frac{1}{n_r} \sum_{i=0}^{G-1} \sum_{j=0}^{G-1} \{i \times j\} \times P(i, j) - \{\mu_X \times \mu_Y\}$ $\sigma_X \times \sigma_Y$
GLRLM		
SRE	Short-run emphasis	$\frac{1}{n_r} \sum_{i=1}^M \sum_{j=1}^N \frac{P(i, j)}{j^2}$
LRE	Long-run emphasis	$\frac{1}{n_r} \sum_{i=1}^M \sum_{j=1}^N P(i, j) * j^2$
LGRE	Low gray-level run emphasis	$\frac{1}{n_r} \sum_{i=1}^M \sum_{j=1}^N \frac{P(i, j)}{i^2}$
HGRE	High gray-level run emphasis	$\frac{1}{n_r} \sum_{i=1}^M \sum_{j=1}^N P(j, j) * i^2$
SRLGE	Short-run low gray-level emphasis	$\frac{1}{n_r} \sum_{i=1}^M \sum_{j=1}^N \frac{P(i, j)}{j^2 * i^2}$
SRHGE	Short-run high gray-level emphasis	$\frac{1}{n_r} \sum_{i=1}^M \sum_{j=1}^N \frac{P(i, j) * i^2}{j^2}$
LRLGE	Long-run low gray-level emphasis	$\frac{1}{n_r} \sum_{i=1}^M \sum_{j=1}^N \frac{P(i, j) * j^2}{i^2}$
LRHGE	Long-run high gray-level emphasis	$\frac{1}{n_r} \sum_{i=1}^M \sum_{j=1}^N P(j, j) * j^2 * i^2$
GLNU	Gray-level nonuniformity	$\frac{1}{n_r} \sum_{i=1}^M \left( \sum_{j=1}^N P(i, j) \right)^2$

Contd...

**Table 3: Contd...**

Features	Complete name	Equation
RLNU	Run length nonuniformity	$\frac{1}{n_r} \sum_{j=1}^M \left( \sum_{i=1}^N P(i, j) \right)^2$
RP	Run percentage	$\frac{n_r}{P(i, j) * j}$
NGLDM	-	-
Coarseness	-	$\left[ \sum_{i=1}^{G_{\max}} \{p_i \cdot s_i\} \right]^{-1}$
Contrast	-	$\left[ \frac{1}{N_0 \cdot (N_0 - 1)} \sum_{i=2}^{G_{\max}} \left\{ \sum_{j=2}^{G_{\max}} \{p_i \cdot p_j \cdot (i - j)^2\} \right\} \right] \cdot \left[ \frac{1}{n} \cdot \sum_{i=2}^{G_{\max}} \{s_i\} \right]$
Busyness	-	$\frac{\sum_{i=1}^{G_{\max}} \{p_i \cdot s_i\}}{\sum_{i=1}^{G_{\max}} \left\{ \sum_{j=1}^{G_{\max}} \{i \cdot p_i - j \cdot p_j\} \right\}}$
GLZLM	-	-
SZE	Short-zone emphasis	$\frac{1}{n_z} \cdot \sum_{i=1}^{G_{\max}} \left\{ \sum_{j=1}^{S_{\max}} \left\{ \frac{p_{i,j}}{j^2} \right\} \right\}$
LZE	Long-zone emphasis	$\frac{1}{n_z} \cdot \sum_{i=1}^{G_{\max}} \left\{ \sum_{j=1}^{S_{\max}} \{p_{i,j} \cdot j^2\} \right\}$
LGZE	Low gray-level zone emphasis	$\frac{1}{n_z} \cdot \sum_{i=1}^{G_{\max}} \left\{ \sum_{j=1}^{S_{\max}} \left\{ \frac{p_{i,j}}{i^2} \right\} \right\}$
HGZE	High gray-level zone emphasis	$\frac{1}{n_z} \cdot \sum_{i=1}^{G_{\max}} \left\{ \sum_{j=1}^{S_{\max}} \{p_{i,j} \cdot i^2\} \right\}$
SZLGE	Short-zone low gray-level emphasis	$\frac{1}{n_z} \cdot \sum_{i=1}^{G_{\max}} \left\{ \sum_{j=1}^{S_{\max}} \left\{ \frac{p_{i,j}}{i^2 \cdot j^2} \right\} \right\}$
SZHGE	Short-zone high gray-level emphasis	$\frac{1}{n_z} \cdot \sum_{i=1}^{G_{\max}} \left\{ \sum_{j=1}^{S_{\max}} \left\{ \frac{p_{i,j} \cdot j^2}{i^2} \right\} \right\}$
LZLGE	Long-zone low gray-level emphasis	$\frac{1}{n_z} \cdot \sum_{i=1}^{G_{\max}} \left\{ \sum_{j=1}^{S_{\max}} \left\{ \frac{p_{i,j} \cdot j^2}{i^2} \right\} \right\}$
LZHGE	Long-zone high gray-level emphasis	$\frac{1}{n_z} \cdot \sum_{i=1}^{G_{\max}} \left\{ \sum_{j=1}^{S_{\max}} \{p_{i,j} \cdot i^2 \cdot j^2\} \right\}$
GLNU	Gray-level nonuniformity	$\frac{1}{n_z} \cdot \sum_{i=1}^{G_{\max}} \left\{ \left[ \sum_{j=1}^{G_{\max}} \{p_{i,j}\} \right]^{-2} \right\}$
ZLNU	Zone length nonuniformity	$\frac{1}{n_z} \cdot \sum_{j=1}^{S_{\max}} \left\{ \left[ \sum_{i=1}^{G_{\max}} \{p_{i,j}\} \right]^{-2} \right\}$
ZP	Zone percentage	$\frac{n_z}{n_v}$

GLCM=Co-occurrence gray-level matrix, GLRLM=Gray-level run length matrix, GLZLM=Gray-level zone length matrix, NGTDM=Neighborhood gray-level difference matrix, NGLDM=Neighborhood gray-level different matrix

high pre/postradiotherapy changes. Wilcoxon signed-rank test revealed that 20 T1W radiomic features vary significantly postradiotherapy. These features are shown in Table 5. On the contrary, ADC features did not vary significantly postradiotherapy. In regard to T2W radiomic features, only five features had significant changes postradiotherapy. The features ENTROPY\_

HISTOGRAM ( $P = 0.004$ ), CONTRAST\_GLCM ( $P = 0.018$ ), ENTROPY\_GLCM ( $P = 0.009$ ), DISSIMILARITY\_GLCM ( $P = 0.02$ ), and CONTRAST\_NGLDM ( $P = 0.013$ ) have undergone significant changes due to radiotherapy. There was no significant correlation between mean radiation dose and radiomic feature changes. Furthermore, no fractures were observed within the follow-up

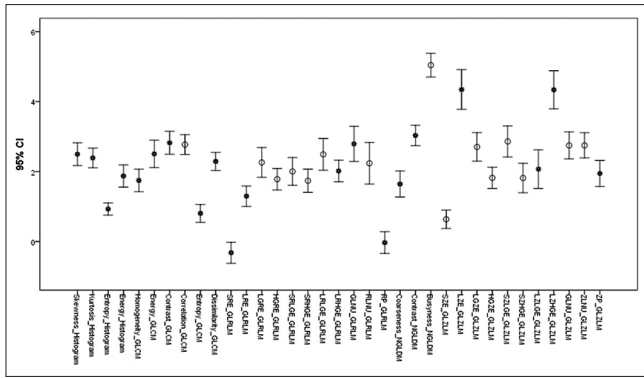


**Figure 2:** T1-weighted radiomic features – percentage Change (normalized) with 95% confidence intervals. Features with significant changes were shown with \*

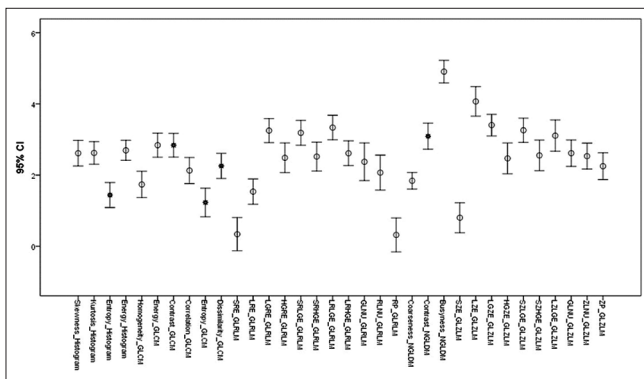


**Figure 3:** T2-weighted radiomic features – percentage change (normalized) with 95% confidence intervals. Features with significant changes were shown with \*

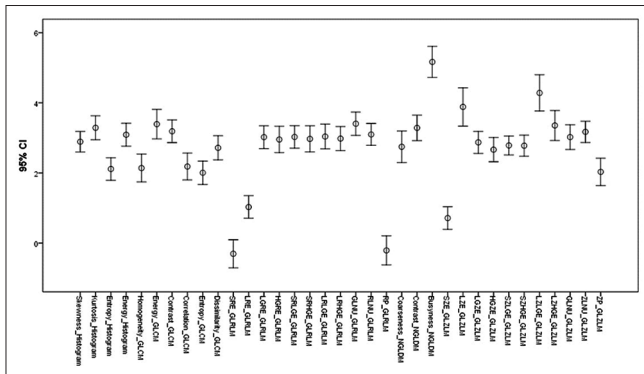


**Figure 4:** Apparent diffusion coefficient radiomic features – percentage change (normalized) with 95% confidence intervals. Features with significant changes were shown with \*

time; hence, the correlation between radiomic feature changes and fracture could not be assessed.

**DISCUSSION**

Radiation-induced bone complications have been observed in different patient populations undergoing radiotherapy.<sup>[23]</sup> In a cohort study, Elliott *et al.* found that the risk of hip fractures

significantly increases up to 76% in 45,662 Pca patients undergoing radiotherapy.<sup>[24]</sup> In another previous retrospective and randomized prospective trials, pelvic insufficiency and hip fractures have been reported in patients treated for pelvic malignancies.<sup>[25]</sup> In this clinical study, we demonstrated the feasibility of radiomic features to assess the radiotherapy-induced femoral head changes. We observed that all selected radiomic features have undergone changes and significant differences in 20 T1 and 5 T2 radiomic features between the pre- and postradiotherapy femoral heads.

In radiomic studies, any feature has its own concept and changes in their values could show structural and functional changes of the tissues being studied. For example, energy is associated with overall homogeneity. In our study, this feature has been changed in the postradiotherapy femoral heads, suggesting changed level of heterogeneity. Furthermore, contrast shows the difference between the highest and the lowest pixel values and is a measure of image local variations. Changes in this feature indicate that image has undergone large variations due to exposure to radiation.

A further finding of our work was that radiomic features obtained from different MR image sequences have different behaviors against radiotherapy. As shown in Figures 2-4, some features had positive percentage changes in T1 and they had negative changes in T2 or ADC and vice versa. A possible explanation for this might be that MRI sequences (T1W/T2W/ADC) have different image acquisition mechanisms and these lead to different image features and feature response.

In recent years, researchers have investigated a variety of MRI for bone diseases detection, characterization, and classification using ADC, but to best of our knowledge, there is no report on the bone ADC feature analysis. In the present work, we showed that radiotherapy induces changes in ADC features, although statistical analysis showed that these changes are nonsignificant. It is also should be considered that *b-value* has a direct impact on ADC features. In our work, we used fixed *b-values* and in future works may use different values to assess radiotherapy-induced damages.

In regard with the role of image feature analysis for bone insufficiency, there are some interesting studies. Nardone *et al.* examined the role of texture analysis (TA) as a predictive factor of radiation-induced insufficiency fractures (IFs). In this study, they performed femoral head computed tomography (CT)-simulation texture analysis of patients undergoing pelvic radiotherapy and concluded that bone CT-TA could be correlated to the risk of radiation-induced IFs.<sup>[26]</sup> They also repeated their work with (3D) TA and found that 3D-bone CT-TA can be used to stratify the risk of the patients to develop radiation-induced IFs.<sup>[27]</sup> In another study, Rachidi *et al.* explored Laws’ masks analysis to describe structural variations of trabecular bone due to osteoporosis on digital radiographs and found that this method constitutes a promising routine



**Table 4: Magnetic resonance imaging radiomic features ranking. Features ranked in the descending order based on median values (absolute). High rank features showing high pre/post radiation therapy changes**

Rank	T1W features	T2W features	ADC features
1	COARSENESS_NGLDM	COARSENESS_NGLDM	SRE_GLRLM
2	LRLGE_GLRLM	LZE_GLZLM	SZE_GLZLM
3	LZLGE_GLZLM	ENERGY_HISTOGRAM	RP_GLRLM
4	ENERGY_HISTOGRAM	ENERGY_GLCM	BUSYNESS_NGLDM
5	HOMOGENEITY_GLCM	LRE_GLRLM	ENTROPY_GLCM
6	SZLGE_GLZLM	SZLGE_GLZLM	LRE_GLRLM
7	RLNU_GLRLM	ENTROPY_HISTOGRAM	RLNU_GLRLM
8	GLNU_GLRLM	SKEWNESS_HISTOGRAM	ZP_GLZLM
9	ZLNU_GLZLM	LRLGE_GLRLM	ENTROPY_HISTOGRAM
10	LRE_GLRLM	ENTROPY_GLCM	HOMOGENEITY_GLCM
11	LZE_GLZLM	CONTRAST_NGLDM	COARSENESS_NGLDM
12	GLNU_GLZLM	LZLGE_GLZLM	HGZE_GLZLM
13	LGZE_GLZLM	GLNU_GLRLM	SRHGE_GLRLM
14	SRE_GLRLM	SRE_GLRLM	DISSIMILARITY_GLCM
15	RP_GLRLM	SRLGE_GLRLM	LGZE_GLZLM
16	ZP_GLZLM	RP_GLRLM	HGRE_GLRLM
17	KURTOSIS_HISTOGRAM	LGRE_GLRLM	LZHGE_GLZLM
18	SKEWNESS_HISTOGRAM	ZP_GLZLM	LZLGE_GLZLM
19	CONTRAST_NGLDM	CONTRAST_GLCM	LGRE_GLRLM
20	HGZE_GLZLM	LGZE_GLZLM	CONTRAST_NGLDM
21	LGRE_GLRLM	SZE_GLZLM	SRLGE_GLRLM
22	ENTROPY_HISTOGRAM	GLNU_GLZLM	LZE_GLZLM
23	SZE_GLZLM	KURTOSIS_HISTOGRAM	SZHGE_GLZLM
24	CORRELATION_GLCM	RLNU_GLRLM	ZLNU_GLZLM
25	CONTRAST_GLCM	HOMOGENEITY_GLCM	CONTRAST
26	SRHGE_GLRLM	SZHGE_GLZLM	ENERGY_HISTOGRAM
27	SZHGE_GLZLM	ZLNU_GLZLM	SZLGE_GLZLM
28	HGRE_GLRLM	HGZE_GLZLM	CORRELATION_GLCM
29	ENERGY_GLCM	CORRELATION_GLCM	KURTOSIS_HISTOGRAM
30	ENTROPY_GLCM	DISSIMILARITY_GLCM	GLNU_GLZLM
31	SRLGE_GLRLM	SRHGE_GLRLM	GLNU_GLRLM
32	LRHGE_GLRLM	BUSYNESS_NGLDM	SKEWNESS_HISTOGRAM
33	DISSIMILARITY_GLCM	HGRE_GLRLM	ENERGY_GLCM
34	BUSYNESS_NGLDM	LRHGE_GLRLM	LRLGE_GLRLM

GLCM=Co-occurrence gray-level matrix, GLRLM=Gray-level run length matrix, GLZLM=Gray-level zone length matrix, NGTDM=Neighborhood gray-level difference matrix, ADC=Apparent diffusion coefficient

technique for the determination of osteoporosis fracture risk from radiographs.<sup>[28]</sup> On the other hand, in a study by Thevenot *et al.*, it was found that femoral neck fracture can be predicted on the basis of clinical radiographs using the combined analysis of bone geometry, textural analysis of trabecular bone, and bone mineral density.<sup>[29]</sup>

Dose–volume effect for radiotherapy-induced femoral head damages has been reported in several studies and some of which indicated that there are no well-established dose constraints for femoral head.<sup>[1]</sup> Emami *et al.* and Bedford *et al.* introduced a 52 Gy tolerance dose for the whole organ and 10% of the organ for probability of complication below 5%, respectively.<sup>[30,31]</sup> In our study, despite the use of IMRT, the mean radiation dose received by femoral head was 40 Gy and there was no correlation between radiation dose and feature changes. In a recent study, Okoukoni *et al.* observed significant postradiotherapy cortical thinning in the intertrochanteric crest of femoral neck. They also identified that there is a correlation between radiation dose and cortical thinning.<sup>[2]</sup>

Based on previous studies and as was reviewed by Zhang *et al.*, due to the different responses of bone cells to radiotherapy

including differentiation and radiosensitivity, the underlying mechanisms are different at different doses.<sup>[32]</sup> However, studies have indicated that, following the radiotherapy, the initial changes in bone result from injury to the remodeling system (osteocytes, osteoblasts, and osteoclasts) which is result of direct irradiation injury to the cells of the remodeling system or the indirect result of irradiation-induced vascular injury, or a combination of both phenomena.<sup>[33]</sup> For radiation-associated fractures, the believed mechanism is radiation-induced vascular fibrosis and impairment of osteoblast cells, which can lead to avascular necrosis and bone atrophy, therefore leaving bone susceptible to fracture.<sup>[34]</sup> There are also some reports associating bone damages with radiation-induced cortical thinning, reduced bone mechanical properties, and reduced bone plasticity.<sup>[35]</sup>

This is the first study to demonstrate the association between radiotherapy-induced femoral head damages and MRI radiomic feature changes and there is a lack of prior research studies on the topic. In similar works, different image texture analyses have been used to assess radiotherapy-induced shrinkage in parotid.<sup>[36,37]</sup> In these studies, a little number of textural features were extracted from CT scanning and

**Table 5: T1W features which had significant changes postradiation therapy**

T1w features	P
LRE_GLRLM	0
LRHGE_GLRLM	0.002
GLNU_GLRLM	0.001
RP_GLRLM	0
COARSENESS_NGLDM	0.002
CONTRAST_NGLDM	0.024
LZE_GLZLM	0
LZLGE_GLZLM	0
LZHGE_GLZLM	0
ZP_GLZLM	0
SKEWNESS_HISTOGRAM	0
KURTOSIS_HISTOGRAM	0.001
ENTROPY_HISTOGRAM	0
ENERGY_HISTOGRAM	0.022
HOMOGENEITY_GLCM	0
ENERGY_GLCM	0
CONTRAST_GLCM	0.02
ENTROPY_GLCM	0
DISSIMILARITY_GLCM	0.001
SRE_GLRLM	0

GLCM=Co-occurrence gray-level matrix, GLRLM=Gray-level run length matrix, GLZLM=Gray-level zone length matrix, NGTDM=Neighborhood gray-level difference matrix

sonography and their results are specific. In comparison to these studies, we extracted several multiparametric MRI radiomic features from different feature categories and our results are different.

Although our results are original and significant, there are limitations associated with this study. First is the number of patients. Future studies will validate our findings on a larger cohort of data. Second is the time of postradiotherapy follow-up. Clinically, radiation-induced femoral head damages often take years to develop after radiotherapy and further long-term follow-up is needed to have more clinically results. However, the present study is a rapid postradiotherapy test and our results indicated that early structural change analysis using radiomic features may contribute to predict postradiotherapy fracture in these patients. Furthermore, these features can be identified as potentially important imaging biomarkers for radiotherapy-induced femoral fractures or any other complications prediction.

## CONCLUSION

MR radiomic feature analysis is a feasible approach for radiotherapy-induced bone damage assessment. These features may be considered as fast, noninvasive, and predictive imaging biomarkers for routine clinical use.

## Financial support and sponsorship

This work was financially supported by Iran University of Medical Sciences, Grant NO. 28744.

## Conflicts of interest

There are no conflicts of interest.

## REFERENCES

- Fiorino C, Valdagni R, Rancati T, Sanguineti G. Dose-volume effects for normal tissues in external radiotherapy: Pelvis. *Radiother Oncol* 2009;93:153-67.
- Okoukoni C, Randolph DM, McTyre ER, Kwok A, Weaver AA, Blackstock AW, et al. Early dose-dependent cortical thinning of the femoral neck in anal cancer patients treated with pelvic radiation therapy. *Bone* 2017;94:84-9.
- Kwon JW, Huh SJ, Yoon YC, Choi SH, Jung JY, Oh D, et al. Pelvic bone complications after radiation therapy of uterine cervical cancer: Evaluation with MRI. *AJR Am J Roentgenol* 2008;191:987-94.
- Iğdem S, Alço G, Ercan T, Barlan M, Ganiyusufoglu K, Unalan B, et al. Insufficiency fractures after pelvic radiotherapy in patients with prostate cancer. *Int J Radiat Oncol Biol Phys* 2010;77:818-23.
- Oh D, Huh SJ, Nam H, Park W, Han Y, Lim DH, et al. Pelvic insufficiency fracture after pelvic radiotherapy for cervical cancer: Analysis of risk factors. *Int J Radiat Oncol Biol Phys* 2008;70:1183-8.
- Shirazi-Fard Y, Alwood JS, Schreurs AS, Castillo AB, Globus RK. Mechanical loading causes site-specific anabolic effects on bone following exposure to ionizing radiation. *Bone* 2015;81:260-9.
- Chandra A, Lin T, Tribble MB, Zhu J, Altman AR, Tseng WJ, et al. PTH1-34 alleviates radiotherapy-induced local bone loss by improving osteoblast and osteocyte survival. *Bone* 2014;67:33-40.
- Szymczyk KH, Shapiro IM, Adams CS. Ionizing radiation sensitizes bone cells to apoptosis. *Bone* 2004;34:148-56.
- Bazzocchi A, Garzillo G, Fuzzi F, Diano D, Albinini U, Salizzoni E, et al. Localizer sequences of magnetic resonance imaging accurately identify osteoporotic vertebral fractures. *Bone* 2014;61:158-63.
- Manenti G, Capuani S, Fanucci E, Assako EP, Masala S, Sorge R, et al. Diffusion tensor imaging and magnetic resonance spectroscopy assessment of cancellous bone quality in femoral neck of healthy, osteopenic and osteoporotic subjects at 3T: Preliminary experience. *Bone* 2013;55:7-15.
- Khoo MM, Tyler PA, Saifuddin A, Padhani AR. Diffusion-weighted imaging (DWI) in musculoskeletal MRI: A critical review. *Skeletal Radiol* 2011;40:665-81.
- Bammer R. Basic principles of diffusion-weighted imaging. *Eur J Radiol* 2003;45:169-84.
- Van Beers BE, Leporq B, Doblaz S, Garteiser P. *Imaging Biomarker Measurements*. Imaging Biomarkers. Cham, Switzerland: Springer; 2017. p. 87-99.
- Aerts HJ, Velazquez ER, Leijenaar RT, Parmar C, Grossmann P, Carvalho S, et al. Decoding tumour phenotype by noninvasive imaging using a quantitative radiomics approach. *Nat Commun* 2014;5:4006.
- Huynh E, Coroller TP, Narayan V, Agrawal V, Hou Y, Romano J, et al. CT-based radiomic analysis of stereotactic body radiation therapy patients with lung cancer. *Radiother Oncol* 2016;120:258-66.
- Cunliffe A, Armato SG 3<sup>rd</sup>, Castillo R, Pham N, Guerrero T, Al-Hallaq HA, et al. Lung texture in serial thoracic computed tomography scans: Correlation of radiomics-based features with radiation therapy dose and radiation pneumonitis development. *Int J Radiat Oncol Biol Phys* 2015;91:1048-56.
- Pota M, Scalco E, Sanguineti G, Farneti A, Cattaneo GM, Rizzo G, et al. Early prediction of radiotherapy-induced parotid shrinkage and toxicity based on CT radiomics and fuzzy classification. *Artif Intell Med* 2017;81:41-53.
- Scalco E, Rizzo G. Texture analysis of medical images for radiotherapy applications. *Br J Radiol* 2017;90:20160642.
- Abdollahi H, Mostafaei S, Cheraghi S, Shiri I, Rabi Mahdavi S, Kazemnejad A, et al. Cochlea CT radiomics predicts chemoradiotherapy induced sensorineural hearing loss in head and neck cancer patients: A machine learning and multi-variable modelling study. *Phys Med* 2018;45:192-7.

20. Shiri I, Rahmim A, Ghaffarian P, Geramifar P, Abdollahi H, Bitarafan-Rajabi A, *et al.* The impact of image reconstruction settings on 18F-FDG PET radiomic features: Multi-scanner phantom and patient studies. *Eur Radiol* 2017;27:4498-509.
21. Saeedi E, Dejkam A, Beigi J, Rastegar S, Yousef Z, Mehdipour A, *et al.* Radiomic feature robustness and reproducibility in quantitative bone radiography: A study on radiologic parameter changes. *J Clin Densitom.* 2018. pii: S1094-6950(18)30070-2.
22. Shiri I, Abdollahi H, Shaysteh S, Mahdavi SR. Test-retest reproducibility and robustness analysis of recurrent glioblastoma MRI radiomics texture features. *Iran J Radiol* 2017;14:e48035.
23. Donneys A, Nelson NS, Perosky JE, Polyatskaya Y, Rodriguez JJ, Figueredo C, *et al.* Prevention of radiation-induced bone pathology through combined pharmacologic cytoprotection and angiogenic stimulation. *Bone* 2016;84:245-52.
24. Elliott SP, Jarosek SL, Alaneer SR, Konety BR, Dusenbery KE, Virnig BA, *et al.* Three-dimensional external beam radiotherapy for prostate cancer increases the risk of hip fracture. *Cancer* 2011;117:4557-65.
25. Baxter NN, Habermann EB, Tepper JE, Durham SB, Virnig BA. Risk of pelvic fractures in older women following pelvic irradiation. *JAMA* 2005;294:2587-93.
26. Nardone V, Tini P, Carbone SF, Grassi A, Biondi M, Sebaste L, *et al.* Bone texture analysis using CT-simulation scans to individuate risk parameters for radiation-induced insufficiency fractures. *Osteoporos Int* 2017;28:1915-23.
27. Nardone V, Tini P, Croci S, Carbone SF, Sebaste L, Carfagno T, *et al.* 3D bone texture analysis as a potential predictor of radiation-induced insufficiency fractures. *Quant Imaging Med Surg* 2018;8:14-24.
28. Rachidi M, Marchadier A, Gadois C, Lespessailles E, Chappard C, Benhamou CL, *et al.* Laws' masks descriptors applied to bone texture analysis: An innovative and discriminant tool in osteoporosis. *Skeletal Radiol* 2008;37:541-8.
29. Thevenot J, Hirvasniemi J, Pulkkinen P, Määttä M, Korpelainen R, Saarakkala S, *et al.* Assessment of risk of femoral neck fracture with radiographic texture parameters: A retrospective study. *Radiology* 2014;272:184-91.
30. Emami B, Lyman J, Brown A, Coia L, Goitein M, Munzenrider JE, *et al.* Tolerance of normal tissue to therapeutic irradiation. *Int J Radiat Oncol Biol Phys* 1991;21:109-22.
31. Bedford JL, Khoo VS, Webb S, Dearnaley DP. Optimization of coplanar six-field techniques for conformal radiotherapy of the prostate. *Int J Radiat Oncol Biol Phys* 2000;46:231-8.
32. Zhang J, Qiu X, Xi K, Hu W, Pei H, Nie J, *et al.* Therapeutic ionizing radiation induced bone loss: A review of *in vivo* and *in vitro* findings. *Connect Tissue Res* 2018;7:1-4.
33. Cunha SSD, Sarmiento VA, Ramalho LM, Freitas AC, Almeida Dd, Tavares ME, *et al.* Effects of radiotherapy on bone tissues. *Radiol Bras* 2007;40:189-92.
34. Pouya F, Kerachian MA. Avascular necrosis of the femoral head: Are any genes involved? *Arch Bone Jt Surg* 2015;3:149-55.
35. Willey JS, Lloyd SA, Nelson GA, Bateman TA. Ionizing radiation and bone loss: Space exploration and clinical therapy applications. *Clin Rev Bone Miner Metab* 2011;9:54-62.
36. Scalco E, Fiorino C, Cattaneo GM, Sanguineti G, Rizzo G. Texture analysis for the assessment of structural changes in parotid glands induced by radiotherapy. *Radiother Oncol* 2013;109:384-7.
37. Yang X, Tridandapani S, Beitler JJ, Yu DS, Yoshida EJ, Curran WJ, *et al.* Ultrasound GLCM texture analysis of radiation-induced parotid-gland injury in head-and-neck cancer radiotherapy: An *in vivo* study of late toxicity. *Med Phys* 2012;39:5732-9.